Design and Additive Manufacturing of a Composite Crossflow Heat Exchanger

T. Mulholland, R. Felber, N. Rudolph
Department of Mechanical Engineering, University of Wisconsin, Madison, WI 53706

Abstract

Additive manufacturing (AM) with composite materials reveals new possibilities for direct manufacturing of end-use products, breaking the paradigm of 3D printing as only a prototyping or pre-production technique that has been the norm for many AM technologies. A crossflow air-to-water heat exchanger (HX) was designed for manufacturing via fused filament fabrication (FFF). Design iterations improved the manufacturability, considering issues such as geometric fidelity, watertightness, print time, support material, and manufacturing cost. Carbon fiber fillers enhanced the thermal conductivity of the base polyamide resin, allowing for thermal HX performance comparable to conventional aluminum finned tube heat exchangers. The anisotropic thermal conductivity impacts the heat exchanger performance. The design and manufacturing challenges reveal additional routes to continued performance gains as the HX is scaled up to an 8 kilowatt product.

Keywords: 3D Printing, FFF, Thermal Conductivity, Additive Manufacturing

Introduction

Material extrusion-based additive manufacturing (AM) technology, such as fused filament fabrication (FFF), is possibly the single largest 3D printing process by number of printers, especially considering the availability of these devices as inexpensive, desktop printers that frequently appear in schools and makerspaces. However, FFF is still widely considered a prototyping technology, and has not yielded many prominent examples of manufactured products, in contrast to AM processes that are used for making shoe soles [1] or printed bones [2].

However, FFF has some unique advantages over other AM technologies that can be exploited to make economically viable manufactured parts. FFF uses low-cost material compared to other technologies. Powder materials can cost $175 to $250 per kg, compared to traditional injection molding materials that cost $2 to $3 per kg [3]. FFF materials, however, cost between $30 and $100 per kg, with the higher price reflecting specialty materials that do not benefit from economies of scale. Moreover, FFF materials will cost much less when production is ramped up, since the production method is the well-known, low-cost plastic extrusion technology. In contrast, powder materials are made through more expensive processes: cryogenic grinding, for example. Because these FFF materials are produced by extrusion, they can also contain high loads of fillers. Powder materials are not suitable for high filler contents, since the separate polymer and filler particles can segregate during powder application. If the filler is incorporated in the powder, it must be extremely short, and the reinforcing or conducting effects of the fibers are minimized. However, FFF materials have been loaded to 40 %vol or higher [4]. This high filler content can allow substantial enhancement of different properties, depending on the filler material, such as strength, stiffness, thermal conductivity, or electrical conductivity.

Finally, FFF machines are substantially less expensive than some other technologies, particularly so for powder-based technologies. While an FFF machine can range from $2500 to $40,000 for a high quality desktop machine up to a mid-range professional machine [5], SLS machines cost $100,000 and upwards [6]. Therefore, if FFF technology is matched with the right combination of material and product, there is a potential for low-cost manufacturing to be viable.

Electrically conductive FFF materials can be made by adding conductive fillers to the base polymer resin, and these have been available for some time. The thermal conductivity can also be enhanced through the addition of fillers, although this generally requires higher filler loads [7] and benefits especially from fillers with a high aspect ratio, such as fibers [8]. It is understood that the fibers will tend to align in the flow direction in injection molding [9], which leads to anisotropic thermal conductivity with the highest conductivities associated with the major flow direction. The same behavior can be expected in the flow direction in FFF processing. These anisotropic properties can influence the design or manufacturing of a part, depending on the application requirements. Thermally conductive polymer composites have been used in injection molding for heat transfer applications, such as heat sinks [8]. However, AM allows parts to be produced with a high geometric complexity without additional costs, and can thus allow some atypical geometries to be manufactured economically. This work focuses on FFF printing of an air-cooled cross-flow heat exchanger, which enhances the heat transfer rate compared to traditional corrugated aluminum heat exchangers by raising the convection coefficient using many pin fins. However, printing these complex geometries yields some manufacturing challenges. Design requirements, manufacturing restrictions, and implications of the anisotropic properties should all be considered for the manufacture of a thermoplastic composite air-cooled heat exchanger.

Methods

Material

A commercially available polyamide material with carbon fiber fillers, called Onyx (Markforged), was used for the print tests in the study. Burnoff tests showed that the material is approximately 14 %wt carbon fiber. The material was characterized by laser flash analysis, to measure the thermal diffusivity, and differential scanning calorimetry, to measure the specific heat capacity, but these measurements are not discussed here; more information is available in [10]. However, the flow-direction thermal conductivity of the Onyx material at room temperature was calculated from these measurements to be approximately 0.9 W/m-K, while the perpendicular conductivity is 0.3 W/m-K, similar to the thermal conductivity of an unfilled polyamide. This anisotropic conductivity has implications that are discussed later.

A Makergear M2 printer, version E was used for printing samples. This FFF printer uses a direct-drive extruder mounted on a gantry with an axis in the x-direction, and the build plate is mobile in the z- and y-directions. A 0.35 mm stainless steel nozzle was chosen for the prints to resist the abrasion caused by the carbon fibers. Since polyamide is hydrophilic, and a high water content can cause printing defects, the material was stored in a dry box with a tube connecting to the printer, allowing the material to be kept dry until printing.

Micro-Computed Tomography (µCT)

Some printed samples were scanned using a Zeiss Metrotom 800 µCT instrument. The technique takes many X-ray images of a sample as it is rotated on a stage; the reconstruction algorithms can convert the many 2D images into a 3D dataset. Scans of small and large printed parts had a resolution in the range of 20 to 40 µm, depending on the size of the object.

Discussion

The heat exchanger (HX) design is shown below in Figure 1. Water enters from one side, flows through half of the internal water channels to the opposite side, where it is recombined in a manifold, then travels through the remaining water channels to reach the outlet. At the same time, air flows perpendicular to the water, through air channels that contain pin fins to enhance the convection coefficient. On the right in Figure 1, the arrangement of airfoil pins through the air channels is shown. Earlier designs began with circular pins, since correlations for flow velocities and heat transfer coefficients are well-known, facilitating the design and verification of the HX. These circular pins very well illustrate some of the problems with using FFF to produce small geometries with sizes on the order of the nozzle diameter, as discussed below.

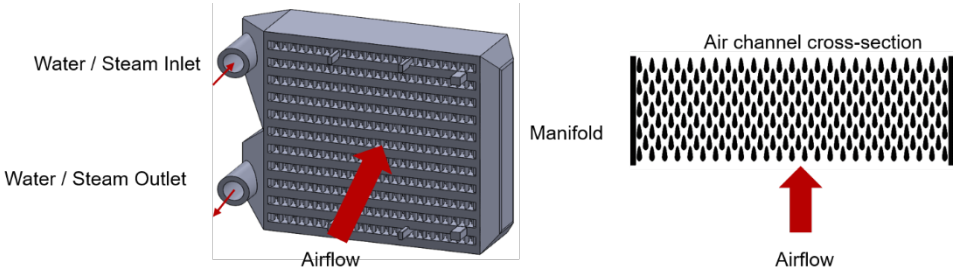

Figure 1. Left: the cross-flow HX with pins and internal water channels. Right: the cross-section of the pins is an airfoil.

To understand the issues with printing small features, it is useful to consider a horizontal cylinder with a diameter equal to the nozzle diameter of the printer: 0.35 mm in this example. When the 3D model is converted into a STereoLithography (STL) file, the surface of the cylinder is tessellated with triangles, and the circle is represented with a series of line segments. This approximation of the circle as a polygon can cause a small loss in the represented circle diameter, which can in turn cause the toolpathing software, known as a slicer, to ignore the feature. To put it another way, some toolpath generation software, such as the free, open-source Slic3r program, will sometimes ignore features that are smaller than a nozzle diameter. Thus, the original 3D model must be slightly enlarged, to account for the loss in diameter during the STL conversion. This is illustrated in Figure 2 below.

As the slicing program creates the 2D layers from the STL file, based on the user-defined layer height (0.10 mm in the example in Figure 2), it will encounter layers containing sections of the cylinder that are thinner than the nozzle diameter. These are ignored, so depending on the quality of the STL file, there may be only one layer that leads to a bead to be printed, illustrated on the right in Figure 2. If this bead is a bridge, like the pin in the example, then the resulting bead will be a small stretched ellipse: quite different from the original, designed cylindrical pin.

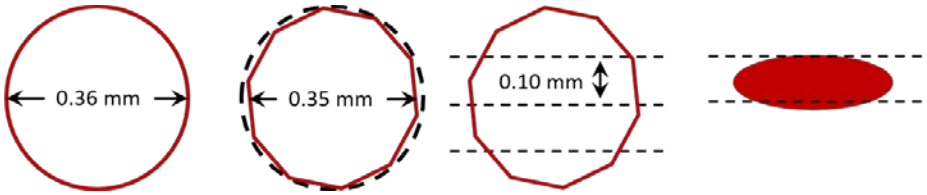

Figure 2. Illustration of geometric losses. Left to right: an axial view of a cylinder designed larger than intended, the STL conversion reduces the circle width, the slicing software divides the shape vertically by layer height, and the only sliced layer wide enough is printed with an elliptical shape.

The pins printed in early versions of the HX were cylinders with a diameter of 1 mm. These cylinders bridge a relatively small gap, between 2 and 3 mm, which is much smaller than the maximum bridge length. Figure 3 shows the maximum packing of beads into the space for the given pin diameter of 1 mm, nozzle diameter of 0.35 mm, and layer height of 0.2 mm. However, if the intended geometry (dashed line) were shifted up slightly with respect to the print layer (i.e. the pin is slightly farther from the build plate), then only seven beads would fit in the space. And as is evident in the µCT image, shown on the right, there is an interaction between the STL file and the toolpath generation that led to only six beads printing in most cases. Regardless, these circular pins do not always consolidate well, leaving holes on the bottom at times, which can lead to disruptions in the airflow, raising the pressure drop in the HX.

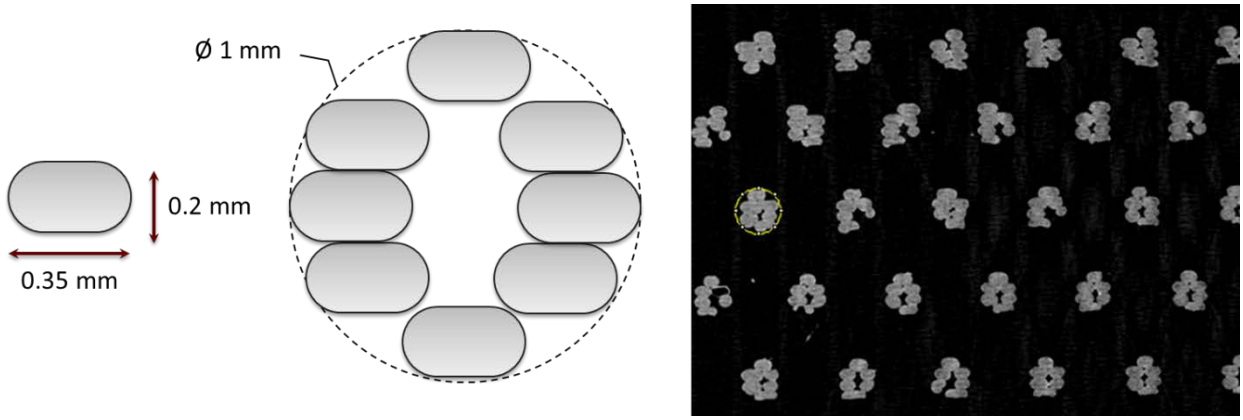

Figure 3. Left: a circular pin as it would be printed with a 0.35 mm nozzle and 0.2 mm layer height. Right: actual circular pins printed with those settings and scanned with µCT.

In order to move to using more complex pin shapes, which were promising for improving the heat transfer per mass and heat transfer per pressure drop ratios, a test piece was designed, which is described in detail in other work [11], as part of this project. The part includes five pin shapes at three different sizes each, as pictured below in Figure 4. The part was printed and scanned via µCT, which allowed some analysis of the geometric fidelity. An example intended cross section of the pins is pictured on the left in Figure 5, whereas the actual print cross section is given on the right; the white color is the material, and the black color is air. Clearly, there are many air gaps in the part, in some cases due to the toolpath (for example, the turns where the pins meet the wall) and in others due to the cross section; where the width of the pin is an uneven multiple of the nozzle diameter, the slicing program ignores the extra space. It is worth noting that these spaces could theoretically be filled, but there is no commercial or open-source slicer known to the author that will do that.

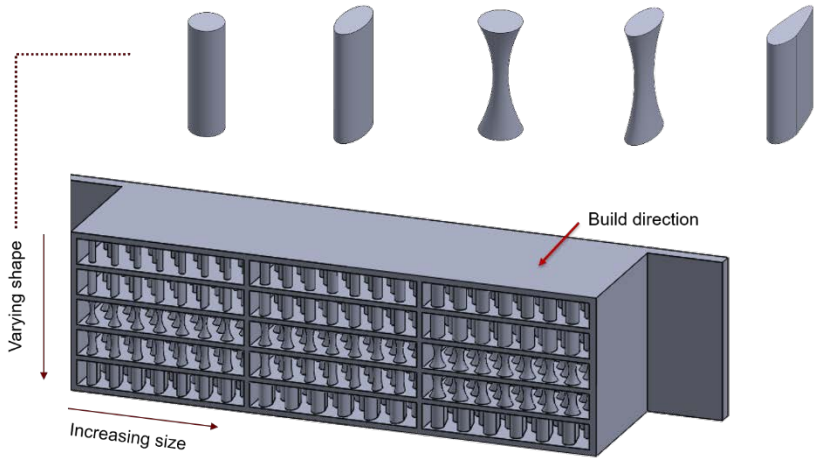

Figure 4. A test piece was designed [11] *to test geometric reproducibility of several fin shapes.*

The airfoil-shaped pins were reproduced fairly well, with few noticeable voids. These are shown in the bottom row of the µCT scan in Figure 5, and a perpendicular cross-section is shown in the bottom row of Figure 6. Although there are some unavoidable voids in the pins, the overall airfoil shape is well-defined. Other shapes, such as the ellipsoids, showed flattening on the top or bottom due to the toolpaths, or poor consolidation, for example in the case of the circular pins.

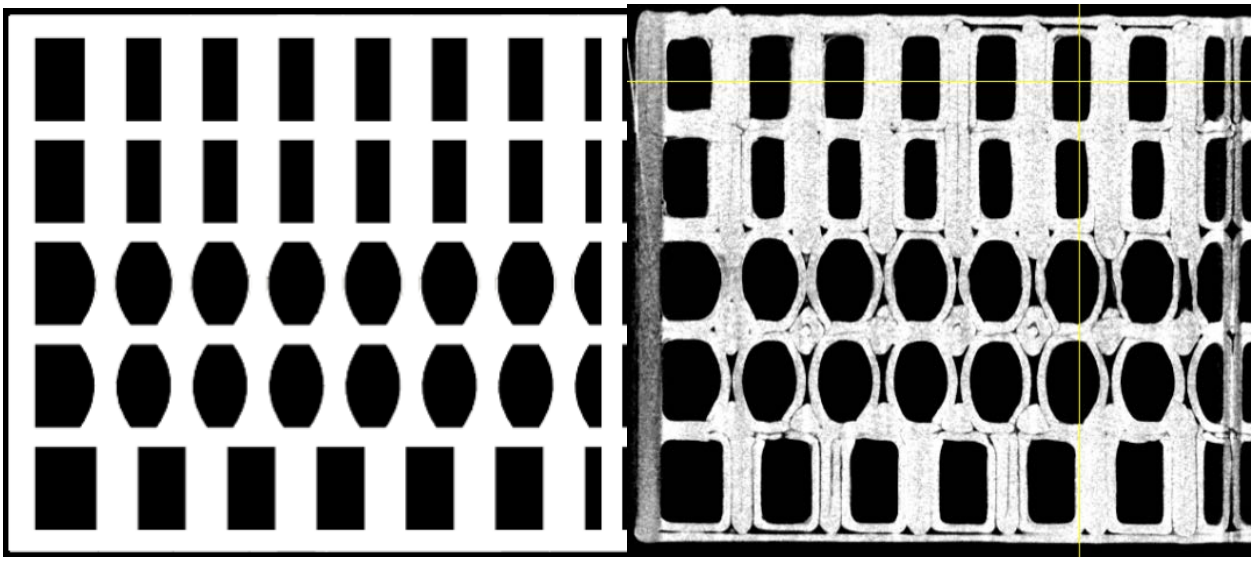

Figure 5. Left: intended xy-plane cross section of the different pin geometries. Right: actual printed geometry showing voids. White represents material and black represents air.

Toolpath issues also affected the walls between the air and water channels, which directly led to a loss of watertightness. Figure 7 shows one of the problems. The left illustration shows toolpaths in red and blue. Examining the blue path, it is seen that the printer produces this geometry by moving in an H-like pattern across the channel, producing the walls and pins simultaneously. In the center image, a closeup view of one pin shows the detailed toolpath at this point. First, the outer edges of the pin are printed. Later, the center of the pin is printed, and a rotational motion attempts to fill the space at the intersection of the pin and wall. This motion reheats the frozen wall and causes deformations, which can lead to holes in the wall. These are shown in Figure 8 on the left.

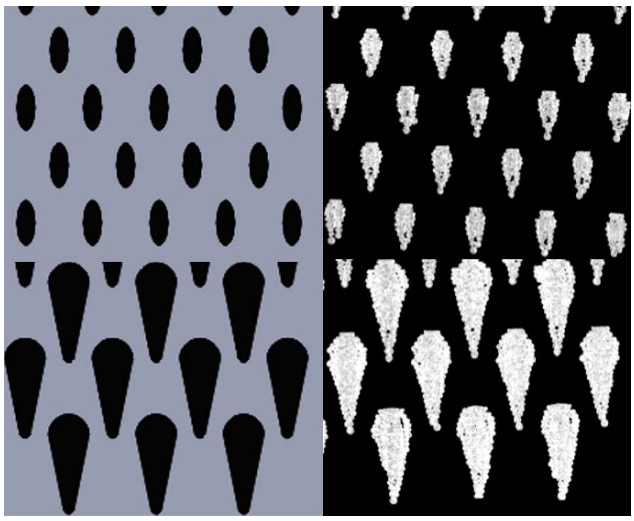

Figure 6. Designed (left) and printed (right) elliptical (top) airfoil (bottom) pins as seen in CT scans.

The right image in Figure 7 shows a custom toolpath, which had to be created by combining separate pin and wall STL files, then assigning a different FFF extruder to each STL. The slicer can be told that the printer has two extruders that occupy the same coordinates, and the tool change-related G-code commands can later be removed. Now, the pin is printed perpendicular to and on top of the previously printed wall, layer by layer. This eliminates the rotational motions at the wall and improves the wall quality, as seen in Figure 8 on the right. Unfortunately, this degree of toolpath control is not currently possible on arbitrary geometries, and there are still imperfect moves in the improved toolpath. For example, the right side of the pin is first printed in space (Figure 7, right), instead of beginning at the wall where it could be anchored.

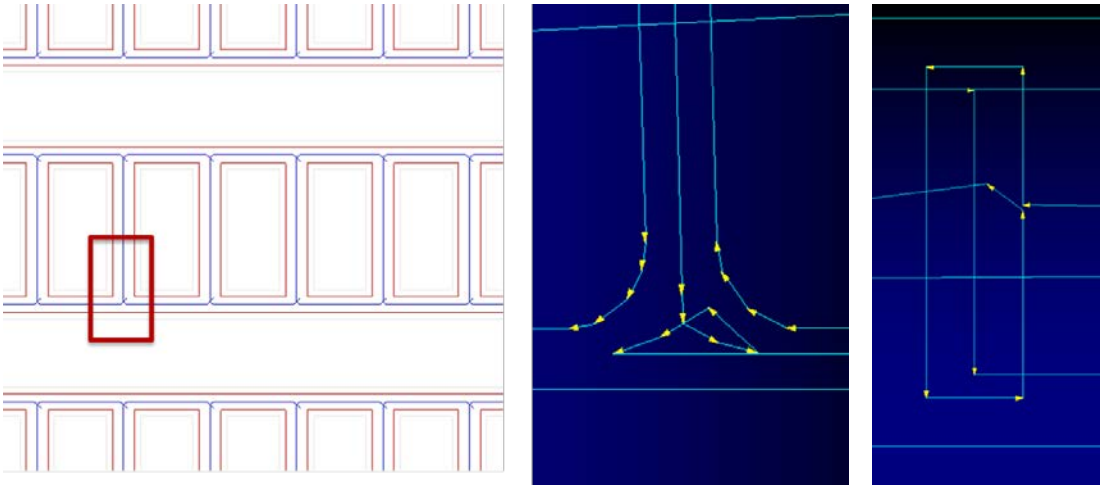

Figure 7. Left: an overview of the pin and wall dividing the air and water channels. Center: inset from left, the unintuitive automatically generated toolpath. Right: a customized, improved toolpath.

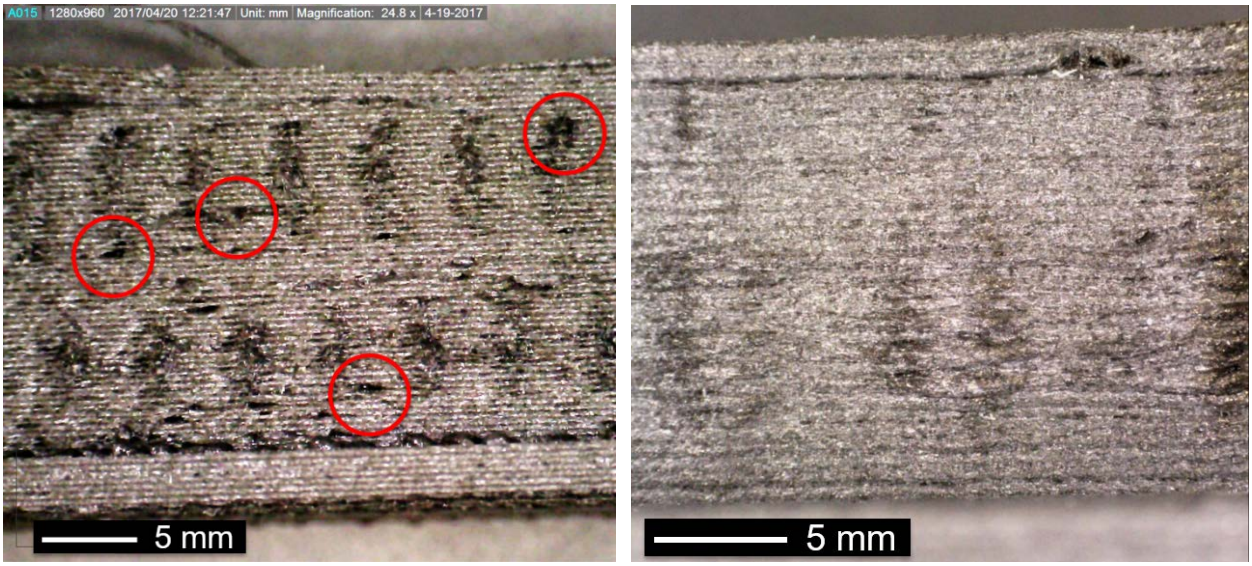

Figure 8. Marks from pin printing can be seen through the wall. Left: The auto-generated slicing path leads to holes in the walls, compromising the watertightness. Right: a custom slicing path improves the wall quality.

When considering the thin walls between the air and water channels, it is also instructive to consider the anisotropic thermal conductivity of a fiber-filled material. Recalling that the thermal conductivity is high in the fiber-aligned direction, which is the same as the flow direction, then the fibers should be aligned along the toolpath in an FFF print.

This presents a fundamental challenge in HX printing; the low conductivity of plastics (even filled plastics) drives the HX design to smaller and smaller features to shorten conductive paths, but small features greatly constrain the possible tool paths. The two most important features in the design are the fins and the walls dividing the two fluids. The fins will ideally conduct heat from the fluid to the walls (in-plane) at a very high rate. However, the walls will ideally conduct heat from one fluid channel into the other (through-plane), but not conduct along the length or width of the wall (in-plane). As illustrated in Figure 9 below, the fibers are oriented in the ideal direction along the axis of the pin, but they are oriented perpendicular to the ideal direction in the walls.

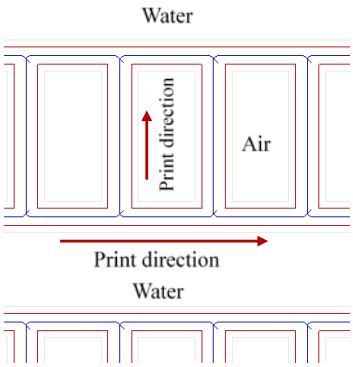

Figure 9. Schematic drawing of the print direction in the walls and fins.

For a given thermal conductivity, the HX wall should be as thin as possible. However, a very thin wall means that the toolpath during printing will be oriented along the length of the wall, putting the fibers in the worst orientation. One alternative could be to print the walls with a

perpendicular path, creating them with S-shapes. This requires thicker walls, which raise the weight of the heat exchanger, so the effect on the overall heat transfer per mass performance is unclear. A better solution might be to use an isotropic material in the walls, and only deposit the fiber-filled material in the pins. Dual material printing like that is greatly facilitated by FFF compared to other technologies. Regardless, it is clear that the thermal anisotropy will affect the heat exchanger design and performance.

Conclusion

Although FFF printers and slicing software continue to advance, there are real manufacturing challenges associated with small features and watertight structures. There is some loss in geometric fidelity during the conversion of solid 3D model to STL, and there is a larger loss when filling a relatively small shape with the elliptical beads associated with FFF. Slicing software does not allow fine control over the toolpath in different areas of a part, so currently, users are stuck with workarounds and tricks to address those problems. Nevertheless, advances have been made improving the quality of thin walls with these pin structures. Finally, although these other issues focus on the small-scale structure of the part, the microstructure also matters; that is, the fiber orientation within the material has an important influence on the part performance in this heat transfer application. This must be considered when designing the part, simulating its performance, and developing a manufacturing scheme for enhanced performance.

Future Work

These manufacturing issues were presented in the context of an air-cooled heat exchanger, but they are relevant for technical parts with a small feature size in general. The predictability of the differences between the designed part and the printed geometry is important, especially considering the functional aspect of the small features, cooling fins in this case; this predictability will probably improve as computer-aided design (CAD) software continues integrating printer control schemes, which is beginning to appear in some products such as SolidWorks and AutoCAD. This integration will hopefully lead to some degree of control or influence over the toolpath, since it is easiest to select features before the model is converted to STL. Desired features would include a print order (walls before pins) to improve watertightness, a preferred print direction (print pins moving in the y-direction before moving in the x-direction) to mitigate stringing or reduce the number of accelerations and the print time, and the ability to set different print parameters in different regions of a part.

At the same time, this project will continue to focus on materials and application development. Armed with an understanding of the design issues, materials will be further developed to raise the thermal conductivity, in the flow direction but especially perpendicular to the flow direction. Many filler materials are potentially viable, from aluminum and copper flakes to carbon fiber and graphite. The relationship between the filler shape and the maximum filler content, limited by nozzle clogging, must be better understood. Variety and predictability in the materials will lead to better product design, which will lead to further examples of FFF-manufactured parts.

Acknowledgements

The authors would like to thank the U.S. Department of Energy ARPA-E for funding.

References

[1] Adidas, "Adidas Futurecraft," 2017. [Online]. Available: http://www.adidas.com/us/futurecraft. [Accessed: 2-Aug-2017].

[2] "3D-printed skull implanted in patient," *UMC Utrecht*, 2014. [Online]. Available: http://www.umcutrecht.nl/en/Research/News/3D-printed-skull-implanted-in-patient. [Accessed: 2-Aug-2017].

[3] M. Cotteleer, "3D opportunity for production: Additive manufacturing makes its (business) case | Deloitte University Press," 2014.

[4] M. Nikzad, S. H. Masood, and I. Sbarski, "Thermo-mechanical properties of a highly filled polymeric composites for Fused Deposition Modeling," *Mater. Des.*, vol. 32, pp. 3448–3456, 2011.

[5] M. Franchetti and C. Kress, "An economic analysis comparing the cost feasibility of replacing injection molding processes with emerging additive manufacturing techniques," *J. Adv. Manuf. Technol.*, vol. 88, pp. 2573–2579, 2017.

[6] M. Molitch-Hou, "Desktop SLS: Industrial 3D Printing for the Masses? > ENGINEERING.com," *Engineering.com*, 2017. [Online]. Available: http://www.engineering.com/3DPrinting/3DPrintingArticles/ArticleID/14316/Desktop-SLS-Industrial-3D-Printing-for-the-Masses.aspx. [Accessed: 31-Jul-2017].

[7] I. A. Tsekmes, R. Kochetov, P. H. F. Morshuis, and J. J. Smit, "Thermal conductivity of polymeric composites: A review," in *2013 IEEE International Conference on Solid Dielectrics (ICSD)*, 2013, pp. 678–681.

[8] S. Amesöder, "Wärmeleitende Kunststoffe für das Spritzgießen," Universität Erlangen-Nürnberg, 2010.

[9] C. Heinle, "Simulationsgestätzte Entwicklung von Bauteilen aus Wärmeleitfähigen Kunststoffen," FAU Erlangen, 2012.

[10] T. Mulholland, A. Falke, and N. Rudolph, "Filled Thermoconductive Plastics for Fused Filament Fabrication," *Proc. Solid Free. Fabr.*, 2016.

[11] R. A. Felber, "Design, simulation, and testing of novel air-cooled heat exchangers manufactured by fused filament fabrication," University of Wisconsin - Madison, 2017.